

A comparative study of MRI-induced RF heating in pediatric and adult populations with epicardial and endocardial implantable electronic devices

Fuchang Jiang, Bhumi Bhusal, Pia Sanpitak, Gregory Webster, Andrada Popescu, Daniel Kim, Giorgio Bonmassar, and Laleh Golestanirad, *Member, IEEE*

Abstract— Patients with congenital heart defects, inherited arrhythmia syndromes, and congenital disorders of cardiac conduction often receive a cardiac implantable electronic device (CIED). At least 75% of patients with CIEDs will need magnetic resonance imaging (MRI) during their lifetime. In 2011, the US Food and Drug Administration approved the first MR-conditional CIEDs for patients with endocardial systems, in which leads are passed through the vein and affixed to the endocardium. The majority of children, however, receive an epicardial CIED, where leads are directly sewn to the epicardium. Unfortunately, an epicardial CIED is a relative contraindication to MRI due to the unknown risk of RF heating. In this work, we performed anthropomorphic phantom experiments to investigate differences in RF heating between endocardial and epicardial leads in both pediatric and adult-sized phantoms, where adult endocardial CIED was the control.

Clinical Relevance—This work provides a quantitative comparison of MRI RF heating of epicardial and endocardial leads in pediatric and adult populations.

I. INTRODUCTION

Cardiac implantable electronic devices (CIEDs) treat cardiac conduction disorders, replacing sinus and atrioventricular nodal function and providing high voltage defibrillation for abnormal heart rhythms in both adults and children [1, 2]. Two types of CIED leads are commonly used in clinical practice depending on patient's body size and venous anatomy: Adults and older children typically receive endocardial systems, with the leads inserted directly through the subclavian vein and the implantable pulse generator (IPG) placed in the left or right subpectoral pocket [3, 4]. Infants and young children often receive an epicardial system, which requires a sternotomy or thoracotomy to sew the cardiac lead directly to the myocardium. The IPG is then usually placed inferior to the abdominal rectus. Although cases of young children being implanted with the endocardial system are rare, there are reports of young patients (< 8 kg) with a transvenous pacing system [4]. Also, for adult patients with residual right-to-left shunts, or those with chambers that cannot be accessed

by the transvenous route, epicardial leads implantation is necessary [5].

At least 75% of patients with CIEDs will require magnetic resonance imaging (MRI) exams during their lifetime [6]. Unfortunately, however, MRI is not readily accessible to patients with electronic implants due to risks associated with the interaction of MRI fields and the implanted device. Since the first report of such harmful effects in 1989 [7] significant improvement has been made in implant design and manufacturing, leading to the first generation of MR-conditional CIEDs that obtained FDA approval in 2011. Such improvements include for example, reduction of ferromagnetic material to reduce the risk of device dislodgement, and enhanced device programming to reduce the risk of unintended tissue stimulation. Tissue heating from radiofrequency (RF) excitation fields, however, remains a major issue. This “antenna effect” happens when the electric field of the MRI transmit coil couples with an elongated conductive lead, causing the specific absorption rate (SAR) of the RF energy to amplify at the lead's tip [8-10]. Consequently, patients with such leads are either contraindicated to receive MRI, or only approved to undergo MRI under strictly controlled conditions.

The Heart and Rhythm Society expert consensus statement on MRI in patients with CIEDs provides Class I recommendation supported by Level A evidence (i.e., strong recommendation supported by high-quality evidence) that patients with MR-conditional CIEDs should only undergo MRI when the product labeling is adhered to [11]. Because FDA-approved MR-conditional labeling is currently only available for CIEDs with endocardial leads, patients with epicardial devices have been mostly excluded from MRI exams [12]. This restriction primarily occurs in the vulnerable pediatric population, or in adults who have congenital heart disease, as the majority of epicardial CIEDs are implanted in children.

The goal of this study was to compare MRI-induced RF heating at tips of epicardial and endocardial leads with realistic trajectories implanted in adult and pediatric

*Research supported by NIH grant R01EB030324.

Fuchang Jiang is with the Department of Biomedical Engineering, Northwestern University, Evanston, IL 60608 USA.

Bhumi Bhusal, Pia Sanpitak, and Daniel Kim are with the Department of Radiology, Northwestern University, Chicago, IL 60611 USA.

Gregory Webster is with the Division of Cardiology, Ann and Robert H. Lurie Children's Hospital of Chicago, Northwestern University Feinberg School of Medicine, 225 East Chicago Avenue, Box 21, Chicago, IL, 60611, USA

Andrada Popescu is with the Division of Medical Imaging, Ann & Robert H. Lurie Children's Hospital of Chicago, Chicago, IL, USA

Giorgio Bonmassar is with the A. A. Martinos Center for Biomedical Imaging, Massachusetts General Hospital, Boston, MA, USA

Corresponding Author: L. Golestanirad is with the Department of Radiology and Department of Biomedical Engineering, Northwestern University, Chicago, IL 60611 USA. Email: laleh.rad1@northwestern.edu

phantoms during MRI at 1.5 T. To our knowledge, such comparative study has not been performed before. Because body size and lead trajectory are two factors that substantially affect RF heating [8, 13-15], we performed experiments in human-shaped phantoms of different sizes implanted with leads that followed patient-derived realistic trajectories. We provide the first preliminary results on RF heating of epicardial leads in clinically relevant populations.

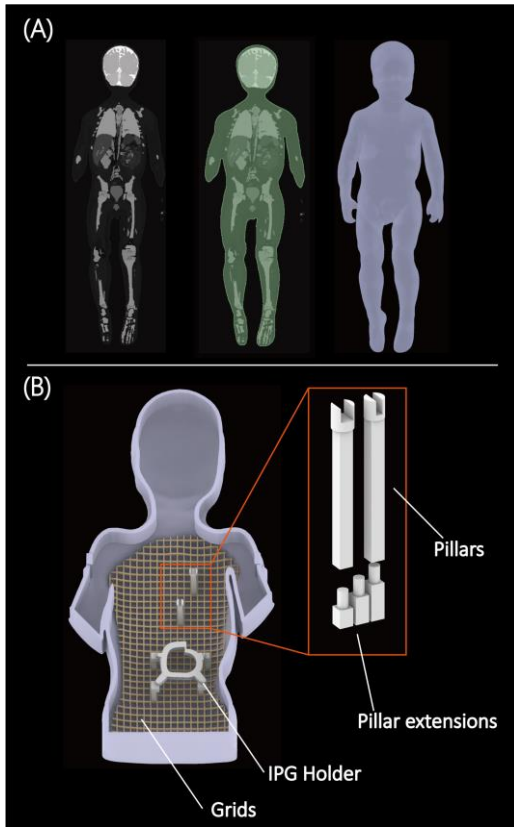


Figure 1. (A) MRI of a 29-month-old child was used to create 3D models of the child's silhouette. (B) Head and torso phantom with grids, pillars, and different height of pillar extensions to adjust the positioning of the CIEDs.

II. METHODS

A. Phantom Design and Construction

Experiments were performed in two human-shaped head-and-torso phantoms representing an adult (length 65 cm, width 45 cm, volume 26 L, weight equivalent value 150lb) and a 29-month-old child (length 53 cm, width 30 cm, volume 11 L, weight equivalent value 30lb). Design and construction of the adult phantom is described elsewhere [16]. The pediatric phantom was designed and 3D printed based on segment MR images of a 29-month-old child [17]. 3D slicer (Slicer 4.10, <http://slicer.org>) was used to smooth segmented MRI masks and create body-shaped surface models [18]. Surface models were further processed in a CAD tool (Rhino 6.0, Robert McNeel & Associates for Windows, Seattle, WA) to create 3D printable objects. We also designed grids, posts, and IPG holders to help positioning CIEDs in well-controlled clinically relevant configurations (Figure 1).

Phantoms were filled with polyacrylamide (PAA) with conductivity of $\sigma = 0.47 S/m$ and relative permittivity of $\epsilon_r = 88$ mimicking average body tissue. We used 9 L and 22 L of PAA to fill the pediatric and adult phantoms, respectively, such that the leads and the IPG were fully submerged at 3 cm depth beneath the surface of the gel (Figure 2).

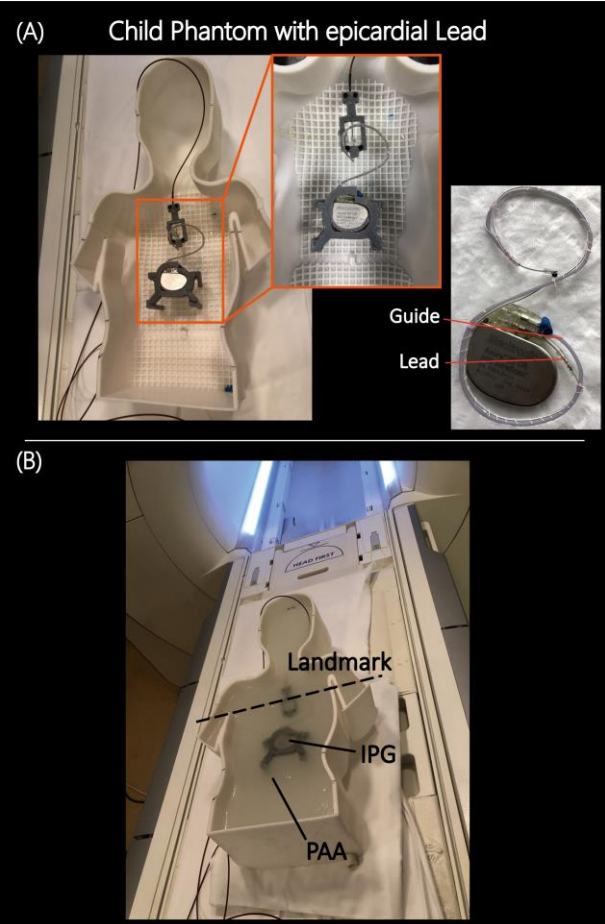


Figure 2. (A) Assembled phantom with CIED and temperature measuring setup before pouring into PAA. 3D printed trajectory guide was attached to the lead (B) Assembled phantom with CIED and temperature measuring setup after pouring into PAA. Chest imaging landmark was used during MR scans.

B. CIED Configurations

Experiments with the epicardial CIED were performed with a 35 cm lead (Medtronic CapSure® EPI 4965) connected to a Medtronic Azure™ XT DR MRI SureScan pulse generator placed in the phantom's abdomen. Experiments with endocardial leads were performed with a 58 cm lead (CapSurFix Novus MRI™ SureScan™ bipolar 5076) connected to the same pulse generator placed in the left infraclavicular region. For each phantom (e.g., child vs. adult), we modeled 5 clinically relevant lead trajectories based on either computed tomography (CT) images of our patients, X-ray images of patients available in the literature, or expert opinion of a pediatric electrophysiologist who implants CIEDs in children and adults (Figure 3).

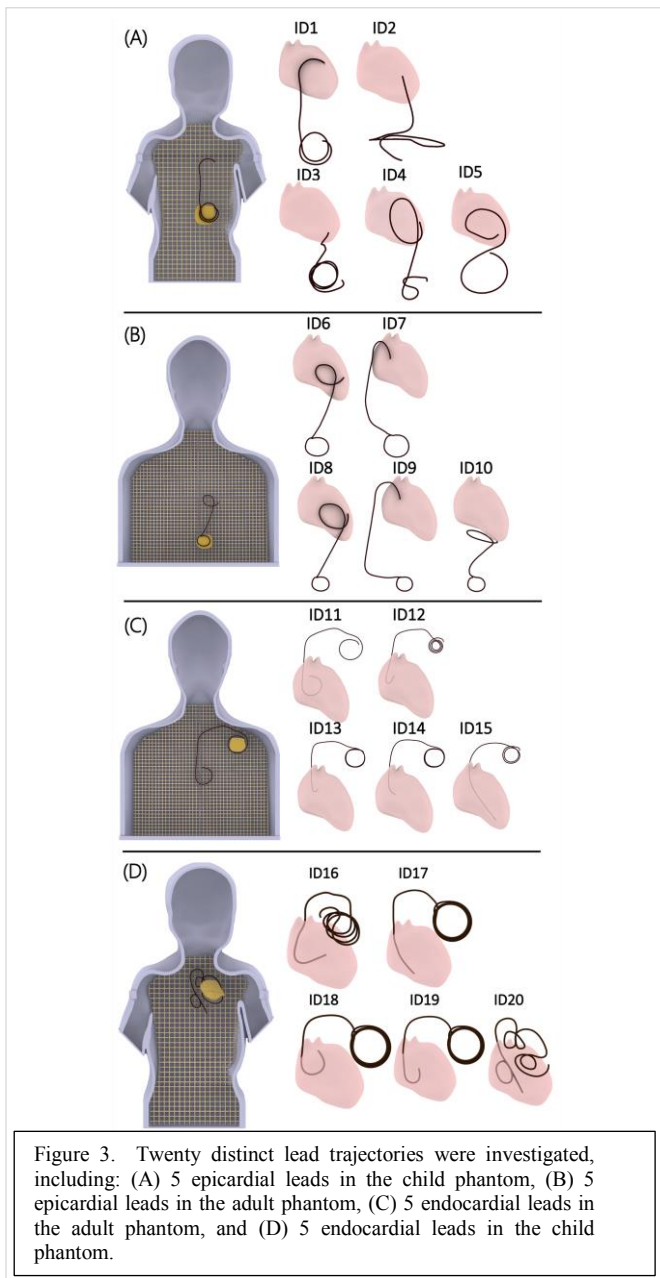


Figure 3. Twenty distinct lead trajectories were investigated, including: (A) 5 epicardial leads in the child phantom, (B) 5 epicardial leads in the adult phantom, (C) 5 endocardial leads in the adult phantom, and (D) 5 endocardial leads in the child phantom.

Temperature measurement was performed using MR-compatible fiber optic probes (OSENSA, Vancouver BC, Canada, resolution 0.01 °C) secured at lead tips. To ensure good thermal contact during experiments, a home-made holder was designed that securely held the probe in contact with the tip of the lead as illustrated in Figure 4.

Measurements were performed in a 1.5 T Siemens Aera scanner (Siemens Healthineers, Erlangen, Germany) with phantoms positioned with the chest at the isocenter. A high-SAR T_1 -weighted turbo spin echo (T_1 -TSE) sequence was used for experiments ($TE=7.3$ ms, $TR=897$ ms, $B_1+=4.9$ μ T, Acquisition time= 280 s).

III. RESULTS

Figure 5 gives the magnitude of RF heating recorded at the tip of each lead after 280 s RF exposure. For each group, the

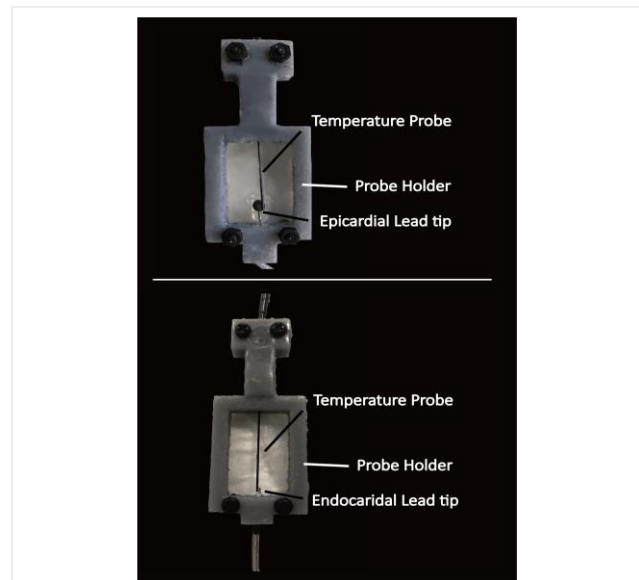


Figure 4. Close view of contact between temperature probe and epicardial/endocardial lead tip.

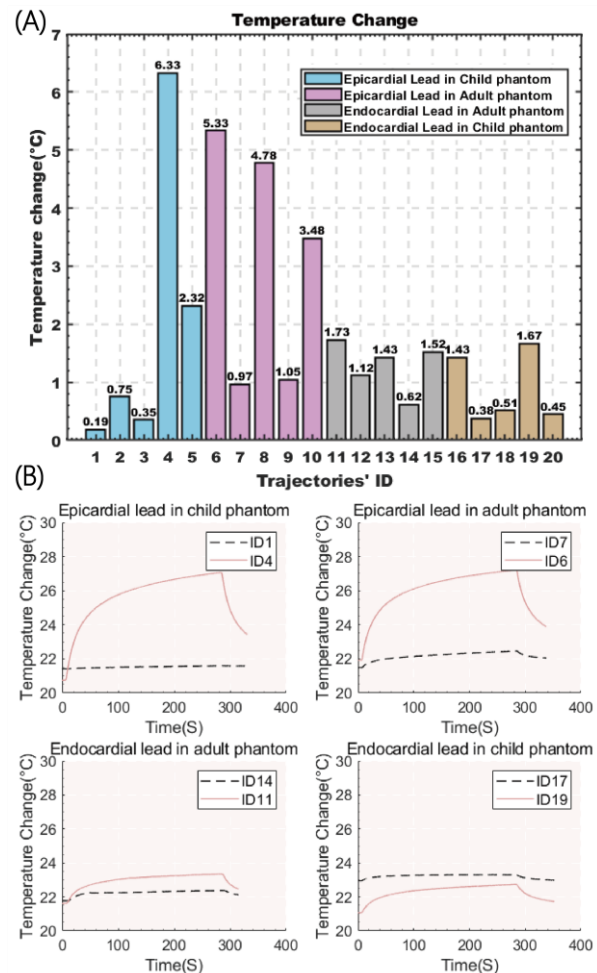


Figure 5. (A) Temperature rise at tips of the lead with 20 different trajectories showed in Figure 3. (B) maximum and minimum of the exponential RF heating measurement for each group

temporal profile of RF heating is also given for cases that generated maximum and minimum heating.

The mean \pm standard deviation of RF heating was 1.99 ± 2.57 °C and 3.12 ± 2.04 °C in pediatric and adult phantoms with the epicardial leads, respectively, and 0.89 ± 0.61 °C and 1.28 ± 0.43 °C in pediatric and adult phantoms with endocardial leads. The highest RF heating was observed in the pediatric phantom with an epicardial lead. Both groups are normally distributed as calculated by the Anderson-Darling normality test ($P>0.05$). A one-tail independent t-test at significant level of $\alpha = 0.05$ showed that epicardial leads generated significantly higher heating compared to endocardial leads (P value = 0.037).

Overall, we observed higher variation in the RF heating of epicardial leads compared to the variation of RF heating of endocardial leads. However, heating is trajectory-dependent as seen in figure 5. This could be explained by the fact that in endocardial CIED implantation, the IPG is consistently placed in the subpectoral pocket and leads are passed through the subclavian vein, which limits the variation in their trajectory. In contrast, there are no rules or guidelines for placing epicardial systems. As a result, surgeons position the IPG and leads based on prior experience and best practices handed from surgeon-to-surgeon, leading to substantial variation in lead trajectories. Because RF heating of an elongated implant highly depends on its trajectory which in turn determines the degree of coupling of the lead with MRI electric fields [19-22], the larger variation in epicardial lead trajectory translates to larger variation in RF heating.

This work did not have enough power to draw inferences as to the effect of body size (i.e., child vs adult) on RF heating. More work is required to establish the safety of MRI in age-specific pediatric populations with epicardial leads.

ACKNOWLEDGMENT

This work was supported by NIH grant R01EB030324.

REFERENCES

- [1] M. Haghjoo, "Chapter 14 - Cardiac Implantable Electronic Devices," in *Practical Cardiology*, M. Maleki, A. Alizadehasl, and M. Haghjoo Eds.: Elsevier, 2018, pp. 251-260.
- [2] L. Gakenheimer-Smith *et al.*, "MRI in pediatric and congenital heart disease patients with CIEDs and epicardial or abandoned leads," (in English), *Pace*, vol. 43, no. 8, pp. 797-804, Aug 2020, doi: 10.1111/pace.13984.
- [3] K. C. Lau, J. W. Gaynor, S. M. Fuller, K. A. Smoots, and M. J. Shah, "Long-term atrial and ventricular epicardial pacemaker lead survival after cardiac operations in pediatric patients with congenital heart disease," (in English), *Heart Rhythm*, vol. 12, no. 3, pp. 566-573, Mar 2015, doi: 10.1016/j.hrthm.2014.12.001.
- [4] J. S. Sachweh *et al.*, "Twenty years experience with pediatric pacing: epicardial and transvenous stimulation," *Eur J Cardiothorac Surg*, vol. 17, no. 4, pp. 455-61, Apr 2000, doi: 10.1016/s1010-7940(00)00364-x.
- [5] M. I. Cohen *et al.*, "Permanent epicardial pacing in pediatric patients - Seventeen years of experience and 1200 outpatient visits," (in English), *Circulation*, vol. 103, no. 21, pp. 2585-2590, May 29 2001. [Online]. Available: <Go to ISI>://WOS:000169012800022.
- [6] R. Kalin and M. S. Stanton, "Current clinical issues for MRI scanning of pacemaker and defibrillator patients," (in English), *Pace*, vol. 28, no. 4, pp. 326-328, Apr 2005, doi: DOI 10.1111/j.1540-8159.2005.50024.x.
- [7] W. Pavlicek *et al.*, "The effects of nuclear magnetic resonance on patients with cardiac pacemakers," *Radiology*, vol. 147, no. 1, pp. 149-153, 1983.

- [8] B. Bhusal *et al.*, "Effect of Device Configuration and Patient's Body Composition on the RF Heating and Nonsusceptibility Artifact of Deep Brain Stimulation Implants During MRI at 1.5 T and 3T," *Journal of Magnetic Resonance Imaging*, vol. 53, no. 2, pp. 599-610, 2021.
- [9] E. Kazemivalipour *et al.*, "Vertical open-bore MRI scanners generate significantly less radiofrequency heating around implanted leads: A study of deep brain stimulation implants in 1.2 T OASIS scanners versus 1.5 T horizontal systems," *Magnetic resonance in medicine*, vol. 86, no. 3, pp. 1560-1572, 2021.
- [10] L. Golestanirad *et al.*, "Changes in the specific absorption rate (SAR) of radiofrequency energy in patients with retained cardiac leads during MRI at 1.5 T and 3T," *Magnetic resonance in medicine*, vol. 81, no. 1, pp. 653-669, 2019.
- [11] J. H. Indik *et al.*, "2017 HRS expert consensus statement on magnetic resonance imaging and radiation exposure in patients with cardiovascular implantable electronic devices," *Heart Rhythm*, vol. 14, no. 7, pp. e97-e153, 2017.
- [12] M. Writing Committee *et al.*, "2021 PACES Expert Consensus Statement on the Indications and Management of Cardiovascular Implantable Electronic Devices in Pediatric Patients: Developed in collaboration with and endorsed by the Heart Rhythm Society (HRS), the American College of Cardiology (ACC), the American Heart Association (AHA), and the Association for European Paediatric and Congenital Cardiology (AEPC) Endorsed by the Asia Pacific Heart Rhythm Society (APHRs), the Indian Heart Rhythm Society (IHRS), and the Latin American Heart Rhythm Society (LAHRS)," *JACC Clin Electrophysiol*, vol. 7, no. 11, pp. 1437-1472, Nov 2021, doi: 10.1016/j.jacep.2021.07.009.
- [13] J. Vu *et al.*, "Machine Learning-Based Prediction of MRI-Induced Power Absorption in the Tissue in Patients With Simplified Deep Brain Stimulation Lead Models," *IEEE Transactions on Electromagnetic Compatibility*, vol. 63, no. 5, pp. 1757-1766, 2021.
- [14] B. Bhusal *et al.*, "Safety and image quality at 7T MRI for deep brain stimulation systems: Ex vivo study with lead-only and full-systems," *Plos one*, vol. 16, no. 9, p. e0257077, 2021.
- [15] P. Nordbeck *et al.*, "Measuring RF-induced currents inside implants: impact of device configuration on MRI safety of cardiac pacemaker leads," *Magnetic Resonance in Medicine: An Official Journal of the International Society for Magnetic Resonance in Medicine*, vol. 61, no. 3, pp. 570-578, 2009.
- [16] B. Bhusal *et al.*, "Effect of Device Configuration and Patient's Body Composition on the RF Heating and Nonsusceptibility Artifact of Deep Brain Stimulation Implants During MRI at 1.5T and 3T," *J Magn Reson Imaging*, vol. 53, no. 2, pp. 599-610, Feb 2021, doi: 10.1002/jmri.27346.
- [17] H. Jeong *et al.*, "Development, validation, and pilot MRI safety study of a high-resolution, open source, whole body pediatric numerical simulation model," *Plos one*, vol. 16, no. 1, p. e0241682, 2021.
- [18] A. Fedorov *et al.*, "3D Slicer as an image computing platform for the Quantitative Imaging Network," (in English), *Magn Reson Imaging*, vol. 30, no. 9, pp. 1323-1341, Nov 2012, doi: 10.1016/j.mri.2012.05.001.
- [19] E. Kazemivalipour *et al.*, "Reconfigurable MRI technology for low-SAR imaging of deep brain stimulation at 3T: Application in bilateral leads, fully-implanted systems, and surgically modified lead trajectories," *NeuroImage*, vol. 199, pp. 18-29, 2019.
- [20] L. Golestanirad *et al.*, "RF-induced heating in tissue near bilateral DBS implants during MRI at 1.5 T and 3T: The role of surgical lead management," *Neuroimage*, vol. 184, pp. 566-576, 2019.
- [21] C. McElcheran *et al.*, "Numerical simulations of realistic lead trajectories and an experimental verification support the efficacy of parallel radiofrequency transmission to reduce heating of deep brain stimulation implants during MRI," *Scientific reports*, vol. 9, no. 1, pp. 1-14, 2019.
- [22] P. Sanpitak *et al.*, "On the accuracy of Tier 4 simulations to predict RF heating of wire implants during magnetic resonance imaging at 1.5 T," in *2021 43rd Annual International Conference of the IEEE Engineering in Medicine & Biology Society (EMBC)*, 2021: IEEE, pp. 4982-4985.